Programmable vector point-spread function engineering

Michael R. Beversluis and Lukas Novotny
The Institute of Optics, University of Rochester, Rochester NY 14627

Stephan J. Stranick
National Institute of Standards and Technology, Gaithersburg, MD, 20899
stranick@nist.gov

Abstract: We use two nematic liquid crystal spatial light modulators (SLM's) to control the vector point spread function (VPSF) of a 1.3 numerical aperture (NA) microscope objective. This is achieved by controlling the polarization and relative phase of the electric field in the objective's pupil. We measure the resulting VPSF's for several different pupil field polarization states. By using single fluorescent molecules as local field probes, we are able to map out the focal field distributions and polarization purity of the synthesized fields. We report the achieved field purity and address the experimental issues that currently limit it.

OCIS codes: (180.6900) Three-dimensional microscopy, (230.6120) Spatial light modulators

References and links

1. B. Richards and E. Wolf, "Electromagnetic diffraction in optical systems II. Structure of the image field in an aplanatic system," Proceedings of the Royal Society of London A **253**, 358–379 (1959).
2. C. J. R. Sheppard and K. G. Larkin, "Vectorial pupil functions and vectorial transfer functions," Optik **107**, 79–87 (1997).
3. R. Dorn, S. Quabis, and G. Leuchs, "Sharper focus for a radially polarized light beam," Phys. Rev. Lett. **91**, 233 901 (2003).
4. G. Toraldo di Francia, "Nuovo pupille superrisolvente," Atti Fond. Giorgio Ronch **7**, 366–372 (1952).
5. C. C. Sun and C. K. Liu, "Ultrasmall focusing spot with a long depth of focus based on polarization and phase modulation," Opt. Lett. **28**, 99–101 (2003).
6. C. J. R. Sheppard and A. Choudhury, "Annular pupils, radial polarization, and superresolution," Appl. Opt. **43**, 4322–4327 (2004).
7. D. P. Biss and T. G. Brown, "Polarization-vortex-driven second-harmonic generation," Opt. Lett. **28**, 923–925 (2003).
8. K. Yoshiki, M. Hashimoto, and T. Araki, "Second-harmonic-generation microscopy using excitation beam with controlled polarization pattern to determine three-dimensional molecular orientation," Jpn. J. Appl. Phys. Part 2 **44**, L1066–L1068 (2005).
9. T. Kuga, Y. Torii, N. Shiokawa, and T. Hirano, "Novel optical trap of atoms with a doughnut beam," Phys. Rev. Lett. **78**, 4713–4716 (1997).
10. L. Novotny, E. J. Sanchez, and X. S. Xie, "Near-field optical imaging using metal tips illuminated by higher-order Hermite-Gaussian beams," Ultramicroscopy **71**, 21-29 (1998).
11. B. Sick, B. Hecht, and L. Novotny, "Orientational imaging of single molecules by annular illumination," Phys. Rev. Lett. **85**, 4482-4485, (2000).
12. L. Novotny, M. R. Beversluis, K. S. Youngworth, and T. G. Brown, "Longitudinal field modes probed by single molecules," Phys. Rev. Lett. **86**, 5251-5254, (2001).
13. S. C. Tidwell, D. H. Ford, and W. D. Kimura, "Generating Radially Polarized Beams Interferometrically," Appl. Opt. **29**, 2234–2239 (1990).
14. E. G. Churin, J. Hossfeld, and T. Tschudi, "Polarization Configurations with Singular Point Formed by Computer-Generated Holograms," Opt. Commun. **99**, 13–17 (1993).

#67705 - $15.00 USD Received 16 February 2006; revised 27 March 2006; accepted 28 March 2006

15. T. Grosjean, D. Courjon, and M. Spajer, "An all-fiber device for generating radially and other polarized light beams," Opt. Commun. **203**, 1–5 (2002).
16. M. Stalder and M. Schadt, "Linearly polarized light with axial symmetry generated by liquid-crystal polarization converters," Opt. Lett. **21**, 1948–1950 (1996).
17. J. A. Davis, D. E. McNamara, D. M. Cottrell, and T. Sonehara, "Two-dimensional polarization encoding with a phase-only liquid-crystal spatial light modulator," Appl. Opt. **39**, 1549–1554 (2000).
18. M. A. A. Neil, F. Massoumian, R. Juskaitis, and T. Wilson, "Method for the generation of arbitrary complex vector wave fronts," Opt. Lett.s **27**, 1929–1931 (2002).
19. M. A. A. Neil, R. Juskaitis, T. Wilson, Z. J. Laczik, and V. Sarafis, "Optimized pupil-plane filters for confocal microscope point-spread function engineering," Opt. Lett. **25**, 245-247 (2000).
20. M. A. A. Neil, R. Juskaitis, M. J. Booth, T. Wilson, T. Tanaka, and S. Kawata, "Adaptive aberration correction in a two-photon microscope," J. Microscopy-Oxford **200**, 105-108 (2000).
21. Certain commerical equipment are indentified in this paper to foster understanding. Such identification does not imply reommendation or endorsement by the National Institute of Standards and Technology, nor does it imply that the equipment identified are necessarily the best available for this purpose.
22. C. Ye, "Construction of an Optical Rotator Using Quarter-Wave Plates and an Optical Retarder," Opt. Eng. **34**, 3031–3035 (1995).
23. B. Richards and E. Wolf, "Electromagnetic diffraction in optical systems I. An integral representation of the image field," Proceedings of the Royal Society of London A **253**, 358–379 (1959).
24. M. Born and E. Wolf, *Principles of Optics* (Cambridge University Press, Cambridge, 1980), sixth edition.

1. Introduction

The quest for higher resolution microscopy leads to the use of high numerical aperture (NA) objectives. One consequence of high NA focusing is that the large marginal ray angles couple transversely polarized fields ($\hat{x}\hat{y}$) within the pupil to focal fields that are polarized along the optical axis ($\hat{z}$) [1]. As a result, the microscope's point spread function is polarization dependent, i.e., a three dimensional vector point-spread function (VPSF) determines the system's resolution capabilities [2]. Furthermore, it has been shown that a tighter focus can be achieved when the incident beam's polarization state has the same cylindrical symmetry as the optical system, for example, when radially polarized beams are used [3]. Additional theoretical work has shown that combining radially polarized beams with Toraldo di Francia annular pupil phase masks [4] generates a focus that is narrower than the diffraction limit of a linearly polarized beam and that has an extended depth of focus [5, 6]. Besides narrower focusing, the fields inside the focus are predominantly polarized along the z-axis, creating strongly enhanced longitudinal fields. These z-polarized focal fields have applications in surface enhanced second-harmonic generation [7, 8], particle-trapping [9], and near-field optical microscopy [10], when the coupling to the surface plasmon resonance of a metal nanostructure is polarization dependent. At issue in this work is the means to create and validate such pupil fields in a configurable and adaptable microscopy system.

To this end, we show that liquid crystal spatial light modulators (SLM's) can be used to control the VPSF of a high NA objective. In order to measure the resulting polarization components of the focus, we have used the technique of using single dye molecules as polarization sensitive local field probes [11, 12]. We found good agreement between the measured and the numerically calculated results.

2. SLM mode-converter

The VPSF can be controlled by creating pupil fields with spatially varying phases and polarizations, such as radially and azimuthally polarized beams. Such modes are typically generated from linearly polarized laser sources using a mode-converter, of which there have been a variety of designs, including polarization interferometers [13], computer generated holograms [14], fiber optics mode couplers [15], passive liquid crystal wave plates [16], and piecewise segmented half-wave plates [3] to perform the necessary polarization rotation across the beam

#67705 - $15.00 USD Received 16 February 2006; revised 27 March 2006; accepted 28 March 2006

profile.

However, these passive devices were limited to a particular polarization mode and to a certain bandwidth around a set center wavelength. To overcome this, Davis *et al* used a liquid crystal spatial light modulator as a two-dimensional polarization encoder [17]. Recently, Neil and coworkers showed that a ferroelectric liquid crystal spatial light modulator could be used as a polarization dependent diffraction grating to produce an arbitrary vector field [18] and Yoshiki *et al* used a spatial light modulator as a controllable polarization rotator in a non-linear microscopy application [8].

Here, we've developed a similar mode-converter that uses a SLM as a spatially addressable optical rotator to control the polarization angle of the objective pupil field. This design is compatible with femtosecond pulsed lasers, and further allows arbitrary phase profiles to be added to the pupil field. The later can be used in applications targeting pupil phase-mask microscopy experiments and for adaptive correction of wavefront distortion in inhomogeneous materials [19, 20]. In this letter, our application is VPSF-engineering, where the SLM mode-converter output beam is coupled to a high NA objective of a microscope, and the resulting control and purity of the VPSF is demonstrated using single molecule fluorescence excitation patterns.

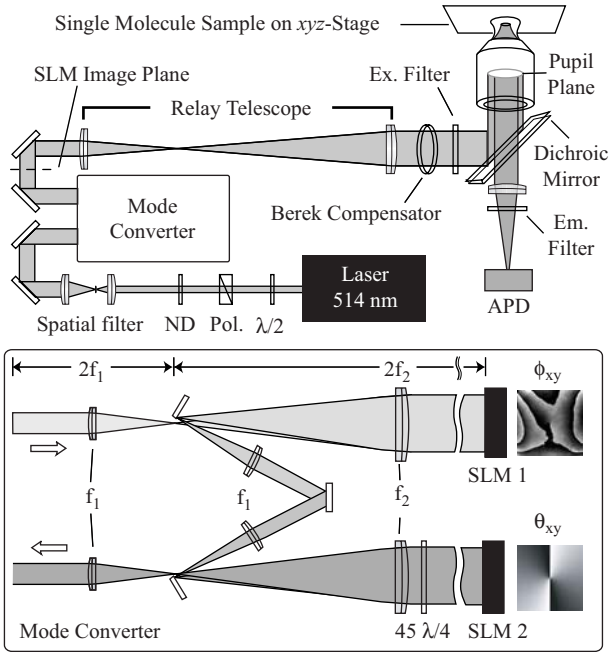

Fig. 1. VPSF experimental schematic drawing using a 1.3 NA oil-immersion objective fluorescence microscope. Each SLM is located in an image plane of the objective's pupil. (ND = Neutral Density filter, Pol. = polarizer, $\lambda/2$ = half-wave plate, $\lambda/4$ = quarter-wave plate, Ex. and Em. = excitation and emission filters, respectively, and APD=Avalanche Photodiode.)

Figure 1 shows the details of the SLM mode-converter. The laser source was a 514 nm Argon-Ion laser. A half-wave plate and a horizontally oriented Glan-Thompson polarizer were used to vary the beam intensity and guarantee high polarization purity. A spatial filter and collimating lens produced a clean, 1 cm diameter TEM_{00} beam, which was directed to the SLM mode-converter.

#67705 - $15.00 USD Received 16 February 2006; revised 27 March 2006; accepted 28 March 2006

The SLM mode-converter controlled the beam's spatial phase and polarization profiles using two Hamamatsu reflective nematic liquid crystal SLM's [21]. Each SLM consisted of a 20 mm square, 768 by 768 element array of horizontally-oriented variable retarders. The elements are optically addressed from behind the liquid crystal substrate, and so there is no physical pixel structure on the SLM. This allows it to have a high reflection without diffractive losses. These elements can be programmed to provide a relative phase shift of 0 to at least 2π for horizontally polarized light for wavelengths between 500 and 1000 nm.

Three telescopes were arranged so that the SLM elements were imaged onto each other and onto the objective pupil, and the telescope magnifications were chosen to match the SLM's clear aperture to the pupil's diameter. The SLMs were slightly tilted around the vertical axis so that their output beams could be picked off with a mirror placed near their telescope's intermediate focus. Consequently, the throughput of this mode-converter is primarily limited by the SLM's 85% reflectance, which yielded a total throughput of 70% for this system.

Each position (xy) on the first SLM generated a pupil field phase $\exp(-i\phi_{xy})$ at its image in the pupil. Likewise, the second SLM was used to piecewise rotate the incident light's polarization state, which was accomplished using a double pass through a $\lambda/4$ wave plate before and after the second SLM [22, 17]. The $\lambda/4$ wave plate was oriented at +45 degrees, and created circular polarization incident on the SLM. After reflecting from the SLM, the vertically-polarized components of this field had been retarded by an amount $\exp(-i\theta_{xy})$ relative to the horizontal components, which in general created an elliptical polarization. The beam was retransmitted through the $\lambda/4$ wave plate, whose mirror image was then effectively oriented at -45 degrees. This caused the polarization to return to its original polarization state (linear) but rotated from the horizontal axis by and angle of $\theta_{xy}/2$. The Jones matrix of this system is:

$$\begin{aligned} T_{xy} &= \frac{\exp(-i\theta_{xy}/2)}{2}\begin{bmatrix} 1 & -i \\ -i & 1 \end{bmatrix}\begin{bmatrix} \exp(-i\theta_{xy}/2) & 0 \\ 0 & \exp(i\theta_{xy}/2) \end{bmatrix}\begin{bmatrix} 1 & i \\ i & 1 \end{bmatrix} \\ &\quad \cdot \begin{bmatrix} \exp(-i\phi_{xy}/2) & 0 \\ 0 & \exp(i\phi_{xy}/2) \end{bmatrix} \qquad (1) \\ &= \exp[-i(\phi_{xy}+\theta_{xy}/2)]\begin{bmatrix} \cos(\theta_{xy}/2) & \sin(\theta_{xy}/2) \\ -\sin(\theta_{xy}/2) & \cos(\theta_{xy}/2) \end{bmatrix} \qquad (2) \end{aligned}$$

Note that the output is a pure coordinate rotation, so that the input polarization state is retained, except for the rotated coordinates. When the SLM mode-converter is used to generate a cylindrical-vector polarized beam, the phase shifting of the first SLM was necessary to compensate for the subsequent residual phase from the polarization rotation by the second SLM. This has also been accomplished by a double reflection from a single SLM [8], but we found that if the beam had more than a few degrees angle of incidence with the SLM's, that this introduced ellipticity in our output beam's polarization. The first SLM phase was also used to subtract the wavefront error resulting from the SLM mode-converter, which totaled 2000 nm peak-to-valley.

After exiting the mode-converter, the output beam profile was imaged into the objective pupil using the third relay telescope. However, before entering the microscope, a variable retarder was placed into the beam to cancel the *s*- and *p*-polarization phase shift of the dichroic mirror used in our fluorescence microscope. This is important because the output of the mode-converter is generally a spatially inhomogeneous mixture of both *s*- and *p*-polarizations. The *s* and *p* Fresnel amplitude coefficients of any reflecting optics after the mode-converter include relative phases which retard these two states, leading to an unwanted elliptical polarizations in the pupil-plane. By aligning the axes of a compensator along the relay optics's *s*- and *p*-axes, the compensator retardation can be set to cancel the accumulated phase.

Once the pupil field distribution was created, single fluorescent molecules were used to image

#67705 - $15.00 USD Received 16 February 2006; revised 27 March 2006; accepted 28 March 2006

the resulting VPSF. This experiment was numerically modeled using Richard's and Wolf's formulas [23, 1] to calculate the expected VPSF. The pupil field is refracted by the objective into a spherical converging wave. This can be modeled as a mapping of the pupil field onto a reference sphere with a radius equal to the objective's focal length. Each point on the sphere corresponds to a spatial frequency component of the focused beam's angular spectrum, whose polarization now lies in a plane tangent to the sphere. Using the mode-converter, the vector can be freely rotated through 2π radians and up to a 2π phase shift can be added relative to the other spatial frequencies. The resulting focal field can be written using a coordinate system origin centered at the focus,

$$\mathbf{E}(\mathbf{r}) \propto \iint_{\Omega} \frac{\mathbf{E}_{ref}(\mathbf{s})}{s_z} e^{i\mathbf{s}\cdot\mathbf{r}} d\mathbf{s} \tag{3}$$

where $\mathbf{r}$ is vector from the origin to an arbitrary point near the focus, $\mathbf{s}$ is a vector of length $2\pi/\lambda$ pointing from the origin towards the converging wave, s_z is the z-component of $\mathbf{s}$ along the optic axis, and the integration is performed over the solid angle Ω contained by the objective's NA. For the images of molecules for different pupil fields, Eq.(2) was used to determine the incident portion of $\mathbf{E}_{ref}$. Because the molecules were placed slightly beneath an air-glass interface, $\mathbf{E}_{ref}$ also included the reflected field from the surface, which can be calculated for each wave vector $\mathbf{s}$ using the appropriate Fresnel equations (we followed the convention given in Born and Wolf's definitions [24]).

3. Experiment

The VPSF was measured using images of single molecule fluorescence excitation patterns. Our single molecule samples were prepared by spin-coating a 0.1 nM DiI dye solution onto a clean glass cover slip. The molecules were then coated with a transparent 20 nm thick poly(methyl methacrylate) film to reduce photobeaching. The laser was focused onto the sample using an infinity corrected 1.3 NA oil-immersion objective, and fluorescence was collected in epi-flourescence mode using the same objective. The dichroic mirror, excitation and emission filter designs were chosen to give good image contrast. A 10 nm wide band pass filter, centered at 515.4 nm, was used to remove longer wavelengths from the laser beam before it enters the microscope. The beam was reflected into the microscope objective using a dichroic with 99.9% reflection at 515 nm and 90% transmission above 545 nm. As was mentioned earlier, dichroic mirror designs such as this one often introduce large relative phase shifts between s and p-polarized fields, which is an important consideration in beams that are inhomogenously polarized. The detected fluorescence was emitted back through the objective and was transmitted by the dichroic mirror. Residual laser scatter was removed using a 550 to 650 nm band pass filter, which corresponds to DiI's emission spectrum. The excitation power at the back aperture of the objective was set to 100 nW.

The fluorescence rate R of a molecule near the laser focus is proportional to the square of the projection of the absorption dipole moment $\mathbf{d}$ along the electric field vector:$R(\mathbf{r}) \propto |\mathbf{d}\cdot\mathbf{E}(\mathbf{r})|^2$. When is $\mathbf{d}$ fixed, then scanning the molecule through the focal region will create a map of the focal fields oriented along $\mathbf{d}$. For a pupil polarized linearly in the $\hat{x}$ direction, the strongest focal field component will be $\hat{x}$-polarized. However, once the NA is larger than 1, the relative strength fields along $\hat{y}$ and $\hat{z}$ becomes significant. Scanning $\hat{x}$, $\hat{y}$, and $\hat{z}$-oriented molecules through the focus will create fluorescence patterns that will match the spatial distribution of these field components within the focus. Molecules oriented along intermediate directions will result in patterns that are related to the electric field distribution of these patterns. Single molecule sample preparation results in a random distribution of orientations, so an image of a region containing many molecules will also contain many different patterns. For the engineered VPSF, the molecule's orientation was assigned based on their appearance in a linearly polarized focus.

#67705 - $15.00 USD Received 16 February 2006; revised 27 March 2006; accepted 28 March 2006

This can be cross-checked by comparing the same molecule's appearance when excited with a second pupil polarization state, to see if the patterns change as expected.

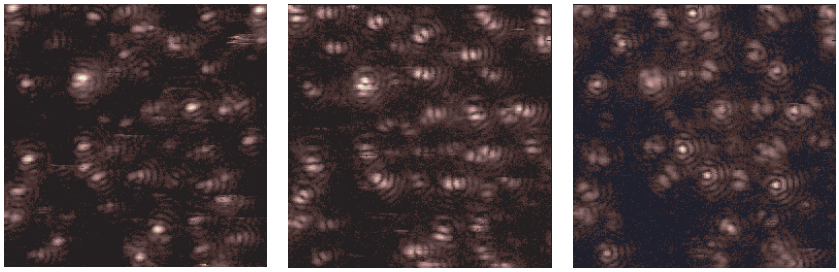

Fig. 2. Successive images of a single molecule sample for pupil polarizations that are: (A) Linear polarized along x (horizontally), (B) azimuthally-polarized, and (C) radially-polarized. The field of view is 10 microns square.

Figure 2 shows a sequence of images taken of the same sample region using different SLM profiles to generate $\hat{x}$-oriented linear-polarized, azimuthally-polarized, and radially-polarized pupil. In Fig 2(A), molecules oriented along $\hat{x}$ appeared as a slightly elongated horizontally-oriented ellipse, while those oriented along $\hat{z}$ appeared as horizontally-oriented twin lobed pattern that is about ten times weaker, and those oriented along $\hat{y}$ appeared as a faint four-lobed cloverleaf pattern, whose intensities are approximately one hundred times weaker than those patterns from molecules oriented along $\hat{x}$. Some molecules were not present in the later images due to photobleaching, but otherwise, the fluorescence patterns in the successive images showed the correct VPSF progression as the pupil polarization is changed from linear polarization to azimuthal and radial modes.

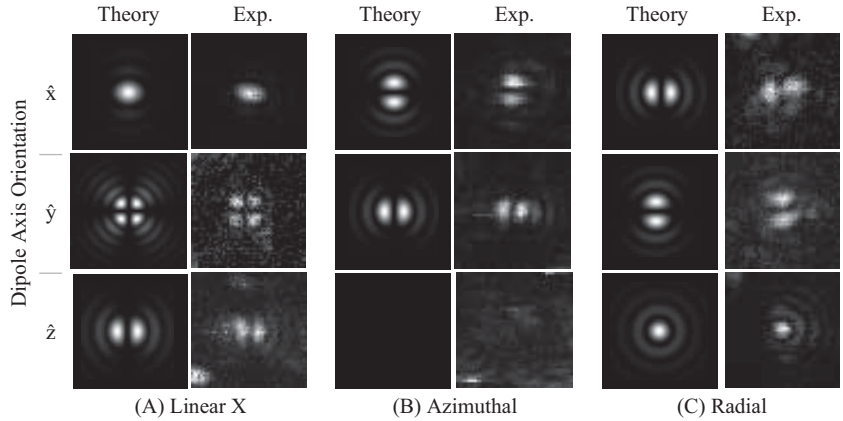

Fig. 3. A comparison of theoretical and experimental images for pupil polarizations that are: (A) Linear along $\hat{x}$, (B) azimuthally-polarized, and (C) radially-polarized. Each image is 2 microns square and has been displayed with a normalized gray scale.

Figure 3 summarizes this progression for $\hat{x}$-, $\hat{y}$-, and $\hat{z}$-oriented molecules for each of the three pupil fields. Each experimental image has been normalized to the image's peak count rate, and is displayed next to a likewise sized and normalized theoretically calculated image for each beam and polarization component. Because the images of these molecules showed

#67705 - $15.00 USD Received 16 February 2006; revised 27 March 2006; accepted 28 March 2006

the correct progression from one polarization state to the next, we conclude that their images directly reflect the $\hat{x}$-, $\hat{y}$-, and $\hat{z}$-polarized components of the VPSF.

The clarity of all three polarization components in Fig. 3(A) indicates that the polarization state of the mode converter's linear output was highly pure. In Fig. 3(B), the donut-like nature of the azimuthal mode created a twin-lobbed pattern whose dark axis is oriented along $\hat{d}$. The azimuthally polarize pupil creates a focus with only $\hat{x}$- and $\hat{y}$-polarized electric fields, and so the intensity of each pattern is determined by **d**'s out of plane projection. In Fig. 2(B) and Fig. 3(B), the azimuthal beam showed good purity as the ratio between the peak count rate in the primary lobes and the average count rate in the central null was more than 30:1.

Figure 3(C) shows the resulting VPSF components for a radially polarized beam. For molecules oriented along $\hat{x}$ and $\hat{y}$, their patterns are similar to the azimuthal pattern but rotated by 90 degrees as expected. However, the radial beam also creates a very strong and symmetric $\hat{z}$-field, which is actually more confined than the primary field component of the linearly polarized pupil. As is evident in Fig. 2(C) the $\hat{z}$-component dominates the total VPSF, and so this beam has slightly better resolution than the linearly $\hat{x}$-polarized beam. A measure of mode converter output quality is further provided by the contrast for the $\hat{z}$-oriented molecule in Fig. 3(B) and 3(C): The ratio of maximum count rates between the radial and azimuthal $\hat{z}$-molecule images is 120:1, which is comparable to the polarization contrast specification of the SLM's (200:1).

Reaching these high polarization contrast ratios required careful attention to the experimental arrangement. In many laser microscopy experiments, a dichroic mirror is used to direct the beam into objective. Because of their design, these mirrors can introduce large phase shifts between the *s*- and *p*-polarized components of an inhomogeneously polarized laser beam. As mentioned earlier, this phase must be eliminated in order to generate the desired VPSF, which was the purpose of the Berek compensator in Fig. 1.

4. Conclusion

In this letter we have demonstrated the use of SLM's for programmable VPSF engineering using single molecule dipole moments to map out the changes in focal field distributions for different pupil polarization states. Although the device is complex, it is very flexible and allows for a wide range of pupil fields to be created. Of particular interest to us is the use of this instrument in near-field microscopy applications, where the VPSF of our microscope can be tailored to better couple excitation sources to the plasmon resonances of metal nanostructures. Furthermore, this mode-converter can be used to rapidly investigate the design of superresolving Toraldo di Franica-style annular phase masks for high-resolution far field microscopy. The compatibility of the SLM-mode converter with ultrafast lasers will allow us to take advantage of nonlinear optical contrast mechanisms to suppress the side-lobe energy in a phase-masked superresolving focus. Based on these applications and those outlined earlier, we feel this device has interest to the microscopy community and for those whose applications require strong longitudinally polarized focal fields.

#67705 - $15.00 USD Received 16 February 2006; revised 27 March 2006; accepted 28 March 2006